Defence Research and   Recherche et développement
Development Canada   pour la défense Canada

DEFENCE R&D **DÉFENSE**

Improved Maneuvering Forces and Autopilot Modelling for the ShipMo3D Ship Motion Library

Kevin McTaggart

Defence R&D Canada – Atlantic

Technical Memorandum
DRDC Atlantic TM 2008-162
September 2008

Canada

This page intentionally left blank.

Improved Maneuvering Forces and Autopilot Modelling for the ShipMo3D Ship Motion Library

Kevin McTaggart

Defence R&D Canada – Atlantic

Technical Memorandum

DRDC Atlantic TM 2008-162

September 2008

Principal Author

Original signed by Kevin McTaggart
_____

Kevin McTaggart

Approved by

Original signed by Neil Pegg
_____

Neil Pegg
Head/Warship Performance

Approved for release by

Original signed by Ron Kuwahara for
_____

J.L. Kennedy
Chair/Document Review Panel

Abstract

ShipMo3D is an object-oriented library with associated user applications for predicting ship motions in calm water and in waves. This report describes improvements to the treatment of hull maneuvering forces and rudder forces within ShipMo3D. A proportional-integral-derivative (PID) autopilot is also introduced to ShipMo3D. Predicted turning circles for the tanker Esso Osaka show good agreement with results from sea trials. Maneuvering predictions based on experimental hull maneuvering force coefficients are better than predictions based on hull coefficients from a regression method.

Résumé

Le ShipMo3D est une bibliothèque de programmes-objets munie d'applications utilisateur connexes qui permettent de prédire les mouvements d'un navire en eaux calmes et dans les vagues. Le présent rapport décrit les améliorations effectuées au traitement des forces de manœuvre de la coque et des forces du gouvernail du ShipMo3D. Le ShipMo3D est également muni d'un autopilote proportionnel, intégral, dérivé (PID). Les cercles de giration prédits pour le pétrolier Esso Osaka démontrent de bonnes similarités avec les résultats des essais en mer. Les prédictions qui reposent sur les coefficients de force de manœuvre des coques expérimentales sont meilleures que les prédictions qui s'appuient sur les coefficients de coque de la méthode de régression.

This page intentionally left blank.

Executive summary

Improved Maneuvering Forces and Autopilot Modelling for the ShipMo3D Ship Motion Library

Kevin McTaggart; DRDC Atlantic TM 2008-162; Defence R&D Canada – Atlantic; September 2008.

Introduction: ShipMo3D is an object-oriented library with associated user applications for predicting ship motions in calm water and in waves. Motion predictions are available in both the frequency domain and the time domain. For predictions in the frequency domain, a ship is assumed to travel with quasi-steady speed and heading in waves. For predictions in the time domain, the ship can be freely maneuvering in either calm water or in waves. This report describes improvements to evaluation of hull maneuvering forces and rudder forces. The report also describes the implementation of a proportional-integral-derivative (PID) autopilot within ShipMo3D.

Principal Results: ShipMo3D now has an improved method for evaluation of hull maneuvering forces based on measured hull maneuvering force coefficients. Also, predicted rudder forces now duely consider incident flow velocities and resulting drag and lift force components. Predicted turning circles for the tanker Esso Osaka show good agreement with results from sea trials. Maneuvering predictions based on experimental hull maneuvering force coefficients are better than predictions based on hull coefficients from a regression method.

Significance of Results: This report concludes the development of Version 1.0 of ShipMo3D and addresses the final concerns that arose during development. It is expected that future revisions to Version 1.0 of ShipMo3D will be limited to minor bug fixes.

Future Plans: Development of a new version of ShipMo3D is progressing, and includes modelling of azimuthing propellers.

Sommaire

Improved Maneuvering Forces and Autopilot Modelling for the ShipMo3D Ship Motion Library

Kevin McTaggart ; DRDC Atlantic TM 2008-162 ; R & D pour la défense Canada – Atlantique ; septembre 2008.

Introduction : Le ShipMo3D est une bibliothèque de programmes-objets munie d'applications utilisateur connexes qui permettent de prédire les mouvements d'un navire en eaux calmes et dans les vagues. Les prédictions de mouvement sont disponibles dans le domaine des fréquences et le domaine temporel. Dans le cas des prédictions dans le domaine des fréquences, il est entendu que le navire navigue à une vitesse quasi constante et qu'il met le cap sur les vagues. Dans le cas des prédictions dans le domaine temporel, le navire peut manœuvrer librement en eaux calmes ou dans les vagues. Le présent rapport décrit les améliorations apportées à l'évaluation des forces de manœuvre de la coque et des forces du gouvernail. Le rapport décrit également l'ajout d'un autopilote proportionnel, intégral et dérivé (PID) au sein du ShipMo3D.

Résultats principaux : Le ShipMo3D est maintenant muni d'une méthode d'évaluation améliorée pour les forces de manœuvre de la coque qui s'appuie sur des coefficients de force mesurés. Par ailleurs, les prédictions des forces du gouvernail prennent maintenant en considération les vitesses de courant incident, la résistance obtenue et les composants de la force de portance. Les prédictions des cercles de giration du pétrolier Esso Osaka démontrent de bonnes similarités avec les résultats obtenus lors des essais en mer. Les prédictions qui reposent sur les coefficients de force de manœuvre des coques expérimentales sont meilleures que les prédictions qui s'appuient sur les coefficients de coque de la méthode de régression.

Importance des résultats : Le présent rapport constitue l'étape finale de l'élaboration de la version 1.0 du ShipMo3D et aborde les dernières questions qui se sont présentées au cours de celle-ci. Il est à prévoir que les prochaines révisions de la version 1.0 du ShipMo3D se limiteront à de simples corrections de bogues.

Travaux ultérieurs prévus : L'élaboration d'une nouvelle version du ShipMo3D est en cours et comprend la modélisation des hélices en azimut.

Table of contents

List of tables

List of figures

This page intentionally left blank.

1 Introduction

ShipMo3D is an object-oriented library with user applications for predicting ship motions in calm water and in waves. Initial ShipMo3D developments [1, 2, 3] were aimed at predicting motions in waves for a ship travelling with quasi-steady speed and heading. ShipMo3D was subsequently extended to predict motions in calm water and in waves for a freely maneuvering ship [4]. This report presents improvements to maneuvering forces introduced in Reference 4. A revised treatment is given for utilization of hull maneuvering coefficients from experiments. Also, a revised treatment of rudder forces is given, which includes changes to rudder-propeller interaction forces. The report also introduces a proportional-integral-derivative (PID) autopilot model. The improvements described in this report are included in ShipMo3D 1.0 [5, 6, 7].

This report includes both relevant theory and validation results. Section 2 gives axes systems and equations of motion used by ShipMo3D. Sections 3 and 4 present improved treatments of hull forces and rudder forces. The PID autopilot is presented in Section 5. Section 6 gives validation of turning circle predictions for the tanker Esso Osaka, and is followed by conclusions in Section 7.

2 Axis Systems and Equations of Motion for ShipMo3D Computations

Various axis systems are used when evaluating the forces and resulting motions for a freely maneuvering ship. Ultimately, the motions of a freely maneuvering ship are given in an earth-fixed axis system shown in Figure 1. The instantaneous heading (to) of the ship is denoted χ and the heading (from) of ocean waves is denoted ν.

Like many seakeeping programs, ShipMo3D evaluates ship forces and resulting motions in translating earth axes, as shown in Figure 2. When ocean waves are present, their direction relative to the ship is given according to Figure 3. For large amplitude motions, forces on the ship can be evaluated using the ship-based axis system of Figure 4 and then transformed to translating earth axes.

When computing ship motions in the time domain, it is necessary to select a suitable nominal heading and nominal speed for orienting the translating earth coordinate system used to solve the ship motions at each time step. Computations with ShipMo3D indicate that the translating earth coordinate system can be oriented based on the instantaneous heading and ship speed along that heading at each time step.

During each time step of a time domain simulation, the forces and resulting accelerations are computed in translating earth axes. The resulting accelerations in earth-fixed
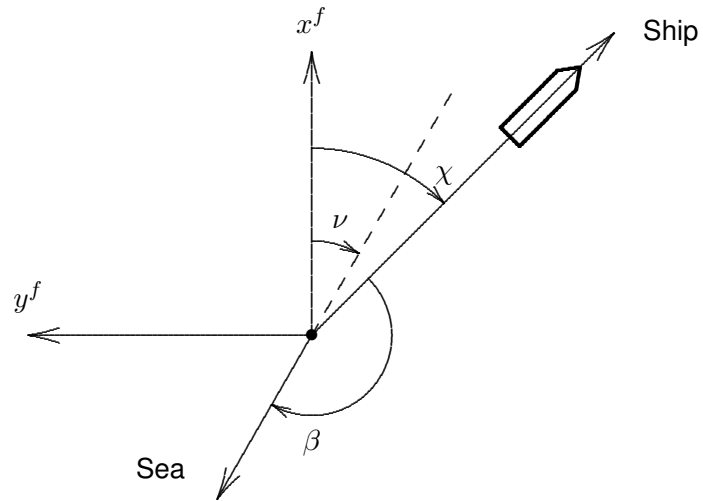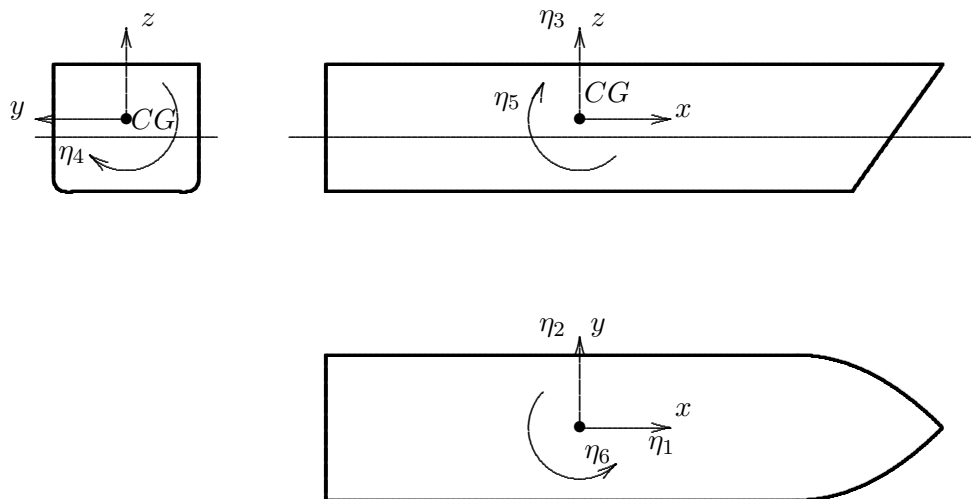
Figure 1: *Earth-Fixed Coordinate System*

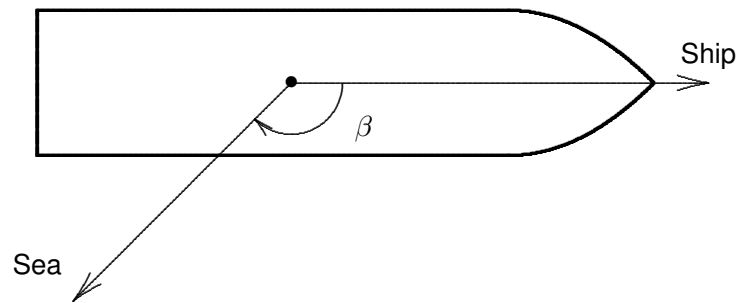**Figure 2:** *Translating Earth Coordinate System*
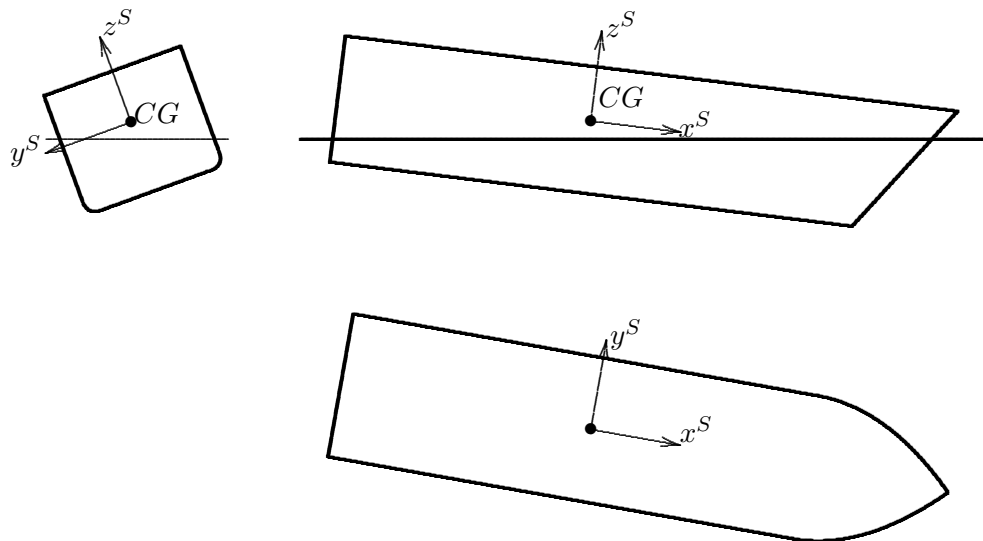
Figure 3: *Sea Direction Relative to Ship*

Figure 4: *Ship Referenced Coordinate System for Large Angular Motions*

axes are:

$$\ddot{x}^f = \ddot{\eta}_1 \cos\chi - \ddot{\eta}_2 \sin\chi \tag{1}$$

$$\ddot{y}^f = -\ddot{\eta}_1 \sin\chi + \ddot{\eta}_2 \chi \tag{2}$$

$$\ddot{\chi} = -\ddot{\eta}_6 \tag{3}$$

Heave, roll, and pitch are equivalent in earth-fixed and translating axis systems.

The equations of motion in the time domain are very similar to those presented in Reference 4. Changes in equations of motion in the current report are due to an integrated approach being used for evaluation of rudder force components. This integrated approach for rudder force components is required to obtain accurate predictions of the significant forces that can act on a rudder in the presence of a propeller. The new equations of motion are:

$$
\begin{aligned}
([M] + [A(U,\infty)])\,\{\ddot{\eta}(t)\} =\ & \\
& - \left[B(U,\infty,\vec{\dot{\eta}})\right]\,\{\dot{\eta}(t)\} - \int_{-\infty}^{t} \left[K^{hull}(U,t-\tau)\right]\,\{\dot{\eta}(\tau)\}\;d\tau \\
& - \left[C(U,\infty,\vec{\dot{\eta}})\right]\,\{\eta(t)\} + \{F^I(t)\} + \{F^D(t)\} + \{F^{cross}(t)\} \\
& + \{F^{resist}(t)\} + \{F^{prop}(t)\} + \{F^{rudder}(t)\}
\end{aligned}
\tag{4}
$$

The ship inertia matrix $[M]$ is based on the dry ship. The added mass matrix $[A(U,\infty)]$ is the infinite frequency value dependent on ship speed U, and includes contributions from the hull and appendages as follows:

$$
\begin{aligned}
[A(U,\infty)] =\ & \left[A^{hull}(U,\infty)\right] + \sum_{i=1}^{N_{foil}} \left[A^{foil-i}\right] + \sum_{i=1}^{N_{rudder}} \left[A^{rudder-i}\right] \\
& + \sum_{i=1}^{N_{skeg}} \left[A^{skeg-i}\right] + \sum_{i=1}^{N_{bk}} \left[A^{bk-i}\right]
\end{aligned}
\tag{5}
$$

where $[A^{hull}]$ is the hull added mass, $[A^{foil-i}]$ is the added mass for static foil i (e.g., propeller shaft bracket), $[A^{rudder-i}]$ is the added mass for rudder i, $[A^{skeg-i}]$ is the added mass for skeg i, and $[A^{bk-i}]$ is the added mass for bilge keel i. The appendage added masses are independent of speed and frequency of motion. The damping matrix includes contributions from the hull and all appendages expect for the rudders as follows:

$$
\begin{aligned}
\left[B(U,\infty,\vec{\dot{\eta}})\right] =\ & \left[b^{hull-rad}(U)\right] + \left[B^{hull-man}(U,\vec{\dot{\eta}})\right] \\
& + \left[B^{hull-visc}(U,|\dot{\eta}_4|)\right] + \sum_{i=1}^{N_{foil}} \left[B^{foil-i}(U,|\dot{\eta}_4|)\right] \\
& + \sum_{i=1}^{N_{skeg}} \left[B^{skeg-i}(U,|\dot{\eta}_4|)\right] + \sum_{i=1}^{N_{bk}} \left[B^{bk-i}(U,|\dot{\eta}_4|)\right]
\end{aligned}
\tag{6}
$$

4

where $[b^{hull-rad}]$ is the hull frequency-independent damping due to potential flow, $[B^{hull-man}]$ is the hull maneuvering damping, which can include forces from lift and cross-flow drag, $[B^{hull-visc}]$ is the hull viscous damping due to roll, $[B^{foil-i}]$ is the damping for static foil i, $[B^{skeg-i}]$ is the damping for skeg i, and $[B^{bk-i}]$ is the damping for bilge keel i. The retardation function matrix $[K^{hull}]$ is due to the dependence of hull hydrodynamic forces on frequency of motion. The stiffness matrix includes contributions from buoyancy, hull potential flow forces, and hull and appendage lift forces as follows:

$$
\begin{aligned}
\left[C(U, \infty, \vec{\eta}) \right] \;=\;& \left[C^{buoy} \right] \;+\; \left[c^{hull}(U) \right] \;+\; \left[C^{hull-man}(U, \vec{\eta}) \right] \\
&+ \sum_{i=1}^{N_{foil}} \left[C^{foil-i}(U) \right] \;+\; \sum_{i=1}^{N_{skeg}} \left[C^{skeg-i}(U) \right] \\
&+ \sum_{i=1}^{N_{bk}} \left[C^{bk-i}(U) \right]
\end{aligned}
\tag{7}
$$

where $[C^{buoy}]$ is the hull buoyancy stiffness, $[c^{hull}]$ is the hull frequency independent stiffness due to potential flow, $[C^{hull-man}]$ is the hull stiffness due to maneuvering forces, $[C^{foil-i}]$ is the lift stiffness for static foil i, $[C^{skeg-i}]$ is the lift stiffness for skeg i, and $[C^{bk-i}]$ is the lift stiffness for bilge keel i. The incident wave excitation vector $\{F^I\}$ consists of the following:

$$
\begin{aligned}
\left\{ F^I(t) \right\} \;=\;& \left\{ F^{I-hull}(t) \right\} \;+\; \sum_{i=1}^{N_{foil}} \left\{ F^{I-foil-i}(t) \right\} \\
&+ \sum_{i=1}^{N_{skeg}} \left\{ F^{I-skeg-i}(t) \right\} \;+\; \sum_{i=1}^{N_{bk}} \left\{ F^{I-bk-i}(t) \right\}
\end{aligned}
\tag{8}
$$

where $\{F^{I-hull}\}$ is the incident wave force on the hull, $\{F^{I-foil-i}\}$ is the incident wave force on foil i, $\{F^{I-skeg-i}\}$ is the incident wave force on skeg i, and $\{F^{I-bk-i}\}$ is the incident wave force on bilge keel i. The wave diffraction force vector $\{F^D\}$ typically only consists of hull forces, unless panelled appendages are included in diffraction computations [3].

Reference 4 describes computation of terms $\{F^{cross}\}$, $\{F^{resist}\}$, $\{F^{prop}\}$ arising from hull cross-flow drag, resistance, and propulsion. The term $\{F^{rudder}\}$ represents all forces acting on the rudders, with the exception of added mass forces that are evaluated on the left hand side of Equation (4). Forces in $\{F^{rudder}\}$ arise from lift and drag, and include effects from rudder deflection, nearby propellers, and water motion in the seaway. Section 4 describes the evaluation of these forces.

Some ship force components are most easily computed using ship-fixed axes, followed by translation to translating earth axes. Figure 4 shows ship-based axes, which can

vary significantly from translating earth axes when motion amplitudes are large. Within ShipMo3D, ship resistance and propulsion forces are assumed to act along the x^S direction of ship-based axes. If buoyancy and incident wave forces are computed using integration of panel pressures in the time domain, then these components are also evaluated using ship-fixed axes.

After selected force components are computed in ship-based axes, they are transformed to translating earth axes using the following:

$$
\begin{aligned}
F_1(t) &= F_1^S(t) \, \cos\eta_5 \, \cos\eta_6 \\
&\quad - F_2^S(t) \, (-\cos\eta_4 \, \sin\,\eta_6 \, + \, \sin\eta_4 \, \sin\eta_5 \, \cos\eta_6) \\
&\quad + F_3^S(t) \, (\cos\eta_4 \, \sin\eta_5 \, \cos\eta_6 \, + \, \sin\eta_4 \, \sin\eta_6) \quad (9) \\
F_2(t) &= F_1^S(t) \, \cos\eta_5 \, \sin\eta_6 \\
&\quad + F_2^S(t) \, (\cos\eta_4 \, \cos\eta_6 \, + \, \sin\eta_4 \, \sin\eta_5 \, \sin\eta_6) \\
&\quad + F_3^S(t) \, (\cos\eta_4 \, \sin\eta_5 \, \sin\eta_6 \, - \, \sin\eta_4 \, \cos\eta_6) \quad (10) \\
F_3(t) &= -F_1^S(t) \, \sin\eta_5 \, + \, F_2^S(t) \, \sin\eta_4 \, \cos\eta_5 \\
&\quad + F_3^S(t) \, \cos\eta_4 \, \cos\eta_5 \quad (11) \\
F_4(t) &= F_4^S(t) \quad (12) \\
F_5(t) &= F_5^S(t) \, \cos\eta_4 \, - \, F_6^S(t)\sin\eta_4 \quad (13) \\
F_6(t) &= F_5^S(t) \, \sin\eta_4 \, + \, F_6^S(t)\cos\eta_4 \quad (14)
\end{aligned}
$$

where F_j is the force for mode j in translating earth axes, and F_j^S is the force for mode j in ship-based axes.

For a ship executing a turning circle, several terms are used to describe the turning circle characteristics, as illustrated in Figure 5. Dimensions are typically referenced to the point at which rudder deflection was initiated. The advance refers to the displacement in the direction of the initial heading, and the transfer refers to the displacement lateral to the the direction of the initial heading. The terms advance and transfer are both often applied to either any point on a turning circle or to the specific point at which the ship heading has changed by 90 degrees relative to the original heading. The tactical diameter is the transfer when the heading has changed by 180 degrees.

3 Evaluation of ShipMo3D Hull Maneuvering Forces from Experimental Coefficients

This section provides an update to hull maneuvering coefficients introduced in Reference 4. ShipMo3D hull maneuvering coefficients do not include forces due to potential
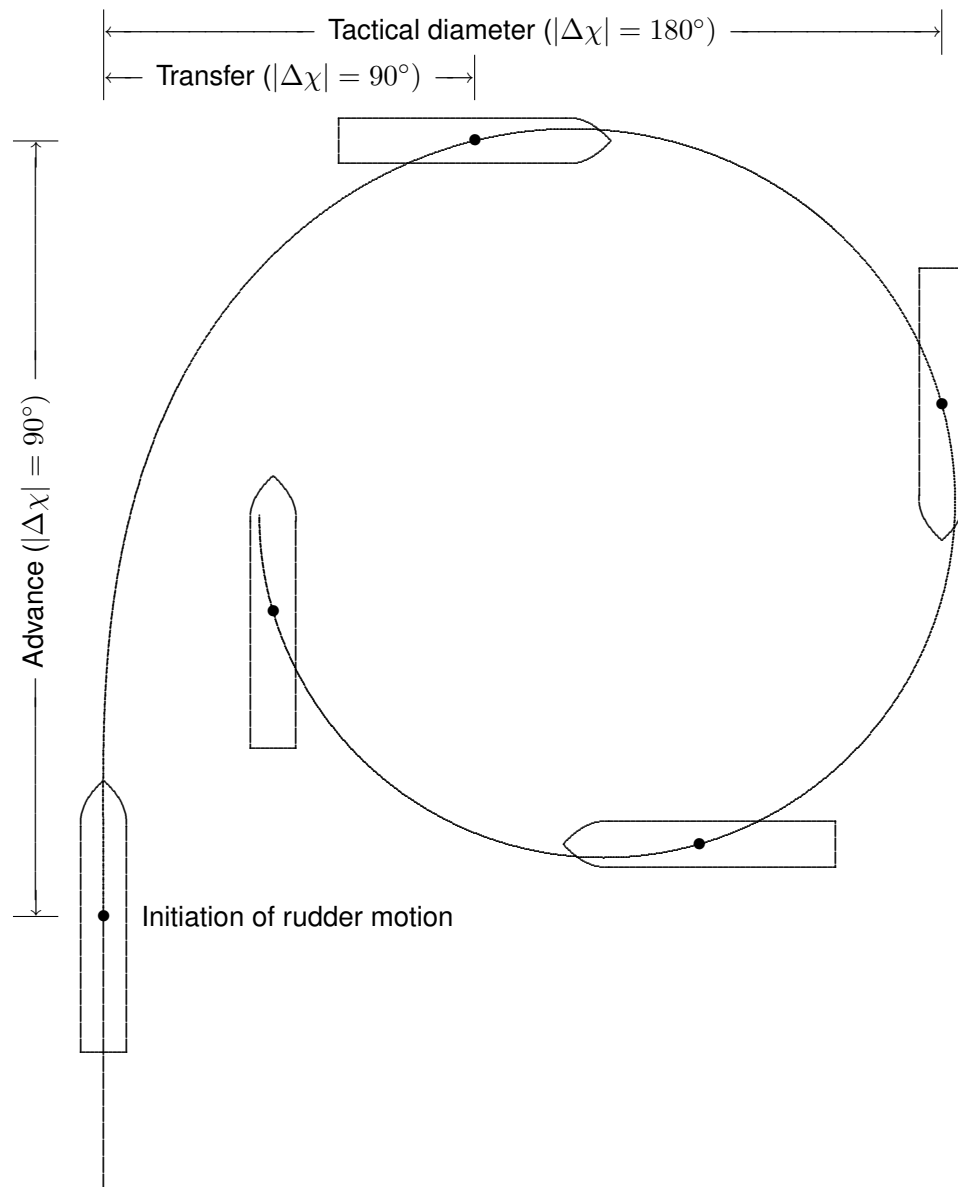
Tactical diameter ($|\Delta\chi| = 180°$)

Transfer ($|\Delta\chi| = 90°$)

Advance ($|\Delta\chi| = 90°$)

Initiation of rudder motion

Figure 5: *Turning Circle Characteristics*

flow; thus, ShipMo3D subtracts potential flow forces from experimentally obtained hull maneuvering coefficients. In Reference 4, it was assumed that experimental hull maneuvering coefficients are measured in translating earth axes at high motion frequencies. In reality, experimental hull maneuvering coefficients are typically measured in stability axes at low motion frequencies. Note that stability axes follow the yaw motions of the ship, as discussed in Schmitke [8].

The formulation for maneuvering coefficients presented previously in Reference 4 assumed that the ship drift angle was small, and the ship forward speed was approximately the same as the total ship velocity in the horizontal plane. It is no longer assumed that drift velocity is small, and ShipMo3D hull maneuvering coefficients are now based on total ship velocity in the horizontal plane, given by:

$$V = \sqrt{(\dot{x}^f)^2 + (\dot{y}^f)^2} \tag{15}$$

Note that total ship velocity is commonly used when defining hull force coefficients in the maneuvering literature [9, 10]. ShipMo3D hull maneuvering coefficients for sway and yaw are consequently now expressed as follows:

$$B_{22}^{hull-man} = V\, B_{22V}^{hull-man} + V\, |v'|\, B_{22V|v'|}^{hull-man} + V\, |r'|\, B_{22V|r'|}^{hull-man} \tag{16}$$

$$B_{26}^{hull-man} = V\, B_{26V}^{hull-man} + V\, |r'|\, B_{26V|r'|}^{hull-man} \tag{17}$$

$$B_{62}^{hull-man} = V\, B_{62V}^{hull-man} + V\, r'^2\, B_{62Vr'^2}^{hull-man} \tag{18}$$

$$B_{66}^{hull-man} = V\, B_{66V}^{hull-man} + V\, |r'|\, B_{66V|r'|}^{hull-man} + V\, v'^2\, B_{66Vv'^2}^{hull-man} \tag{19}$$

The non-dimensional sway velocity v' is given by:

$$v' = \frac{\dot{\eta}_2}{V} \tag{20}$$

The non-dimensional yaw rate is given by:

$$r' = \frac{\dot{\eta}_6\, L}{V} \tag{21}$$

ShipMo3D hull maneuvering force coefficients are evaluated using non-dimensional force coefficients based on Inoue et al. [10]. The linear force coefficients in Equations 16 to 19 are given by:

$$B_{22V}^{hull-man} = -\frac{1}{2}\, \rho\, L\, T_{mid}\, Y_v' - B_{22U}^{hull-rad-stab}(\omega_e = 0) \tag{22}$$

$$B_{26V}^{hull-man} = -\frac{1}{2}\, \rho\, L^2\, T_{mid}\, Y_r' - B_{26U}^{hull-rad-stab}(\omega_e = 0) \tag{23}$$

$$B_{62V}^{hull-man} = -\frac{1}{2}\, \rho\, L^2\, T_{mid}\, N_v' - B_{62U}^{hull-rad-stab}(\omega_e = 0) \tag{24}$$

$$B_{66V}^{hull-man} = -\frac{1}{2}\, \rho\, L^3\, T_{mid}\, N_r' - B_{66U}^{hull-rad}(\omega_e = 0) \tag{25}$$

where ρ is water density, L is ship length between perpendiculars, and T_{mid} is draft at midships. The non-dimensional force coefficients Y'_v, Y'_r, N'_v, and N'_r include both viscous and potential flow effects. The terms $B_{22U}^{hull-rad-stab}$, $B_{26U}^{hull-rad-stab}$, $B_{62U}^{hull-rad-stab}$, and $B_{66U}^{hull-rad-stab}$ are potential flow terms in stability axes, which are included in experimentally measured force coefficients. These terms are subtracted when obtaining maneuvering force coefficients for ShipMo3D because ShipMo3D already considers the potential flow forces. The hull radiation damping terms to be subtracted from the above equations are based on coefficients presented in Reference 2, with terms here given for stability axes:

$$B_{jkU}^{hull-rad-stab}(\omega_e = 0) \quad = \quad -\frac{\partial \widetilde{A}_{jk}^{hull}(U = 0, \omega_e = 0)}{\partial x} \tag{26}$$

where $\partial \widetilde{A}_{jk}^{hull}/\partial x$ is determined from the x derivative of potentials giving added mass with $U = 0$ denoting zero forward speed and $\omega_e = 0$ denoting zero encounter frequency.

4 Rudder Forces

This section gives revisions to the treatment of rudder forces presented previously in References 3 and 4. These revisions are based partly on material presented in recent books by Lewandowski [11] and Faltinsen [12]. Several aspects of modelling of rudder forces have been revised. ShipMo3D previously considered rudder forces to have separate force contributions from ship forward speed and the flow induced by the propeller. This previous treatment has been replaced by an integrated approach that considers both the ship forward speed and the flow induced by the propeller when evaluating the flow incident to the rudder and the resulting total force. When evaluating the lateral flow incident to the rudder, ShipMo3D can now include the flow straightening effects due to the presence of the hull and propellers, which can cause a significant reduction in the lateral velocity of incident flow. Another significant revision is the treatment of rudder lift and drag forces. It was previously assumed that the total force acting on the rudder was due to lift forces acting normal to the rudder. This approach is used in other manuevering models, such as those in References 9 and 13. ShipMo3D now uses the approach described by Newman [14], whereby lift forces act perpendicular to incident rudder flow and drag forces act parallel to incident rudder flow. Limits on lift and drag forces at high angles of attack are also now included in ShipMo3D.

4.1 Lift and Drag Forces on Rudders

Lift and drag forces acting on a rudder are shown in Figure 6. The lift force acts perpendicular to the incident flow V_r, while the drag force acts in the same direction

as the incident flow V_r. The lift force is given by:

$$F_{lift}^{rudder} = \frac{1}{2} \rho S V_r^2 C^{lift}(\alpha) \qquad (27)$$

where S is the rudder area, V_r is the incident flow velocity, C^{lift} is the lift force coefficient, and α is angle of attack between the incident flow and the rudder. At small angles of attack, the lift curve slope $\partial C^{lift}/\partial \alpha$ is linear and can be evaluated based on Whicker and Fehlner [15], as discussed in Reference 3. To account for the influence of stall effects, ShipMo3D places a limit on the maximum lift coefficient of a rudder. Data presented in Reference 16 indicate that a value of 1.2 is a suitable nominal limit for the absolute value of the lift coefficient.
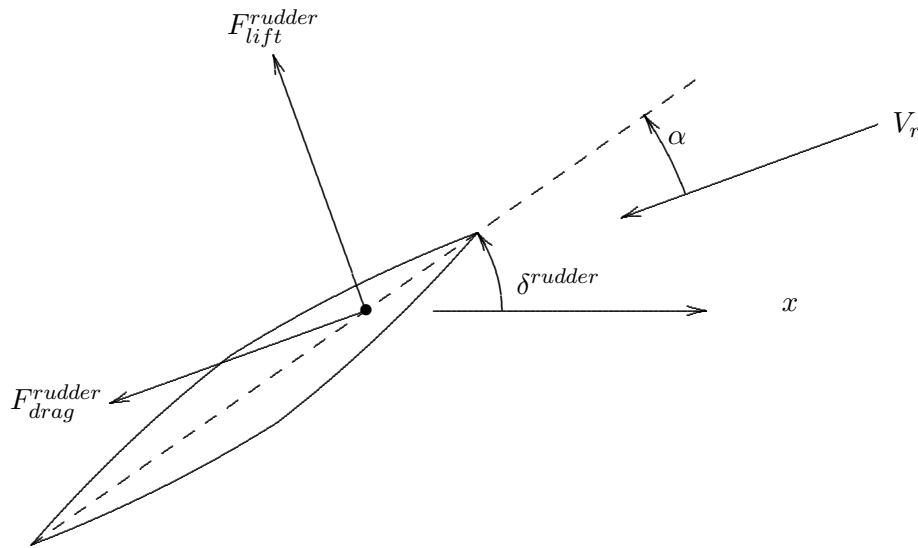
Figure 6: *Lift and Drag Forces Acting on a Deflected Rudder in Incident Flow*

The drag force acting on the rudder is given by:

$$F_{drag}^{rudder} = \frac{1}{2} \rho S V_r^2 C^{drag} \qquad (28)$$

Bertram [16] and Lewandowski [11] indicate that the drag coefficient is proportional to α^2 at low angles of attack, and can be represented as follows:

$$C^{drag} = \alpha^2 \frac{\partial C^{drag}}{\partial(\alpha^2)} \qquad (29)$$

$$\frac{\partial C^{drag}}{\partial(\alpha^2)} = \left(\frac{\partial C^{lift}}{\partial \alpha}\right)^2 \frac{1}{\pi a_e} \qquad (30)$$

For a rudder truncated at the hull, the effective aspect ratio a_e is equal to $2s/\bar{c}$, where s is the rudder span and $\bar{c}$ is the mean chord length. To model the influence of large angles of attack, ShipMo3D applies a limiting value to the drag coefficient of a rudder. A suggested limiting value for the drag coefficient can be based on flow normal to a flat plate, which has a drag coefficient of 1.17.

4.2 Rudder Incident Flow Velocities and Resulting Forces

The most challenging aspect of computing rudder forces is the evaluation of the incident flow into the rudder. When evaluating the incident flow, it is essential to consider ship motions, the presence of the ship hull, and the presence of propellers.

For the present analysis, rudder velocity components u_r, v_r, and w_r will be considered, which are velocities of the rudder relative to the surrounding fluid. The signs of these components are the same as for the x, y, and z coordinates in the translating earth axes of Figure 2. For simplicity, the present discussion assumes small ship motion angular displacements; however, computations within ShipMo3D evaluate rudder forces in ship-based axes and transform them to translating earth axes. Unlike much of the maneuvering literature, the present discussion considers rudders with arbitrary orientation rather than just conventional rudders that are oriented downward from the hull.

The effective longitudinal inflow velocity considers the presence of propellers, and is evaluated using the following equation based on Faltinsen [12]:

$$u_r = \sqrt{\left(1 - \sum_{j=1}^{N_{prop}} C_j^{rudder-prop}\right) U^2 \left(1 - \tilde{w}_r\right)^2 + \sum_{j=1}^{N_{prop}} C_j^{rudder-prop} u_{slip-j}^2} \quad (31)$$

where N_{prop} is the number of propellers, $C_j^{rudder-prop}$ is the rudder-propeller interaction coefficient from propeller j, U is the ship forward speed, $\tilde{w}_r$ is the rudder wake fraction, and u_{slip-j} is the velocity of the propeller slipstream at the rudder. The rudder-propeller coefficient $C^{rudder-prop}$ will have a value approximately equal to the fraction of rudder area within the propeller slipstream. The velocity of the propeller slipstream can be evaluated from Bertram [16] based on original work by Söding [17, 18]. The flow velocity far aft of the propeller based on potential flow is given by:

$$u_{slip}^{\infty} = U \left(1 - \tilde{w}_{prop}\right) \sqrt{1 + C_{th}} \quad (32)$$

where $\tilde{w}_{prop}$ is the propeller wake fraction. The propeller thrust loading coefficient C_{th} is given by:

$$C_{th} = \frac{F^{prop}}{1/2\, \rho\, U^2 \left(1 - \tilde{w}_{prop}\right)^2\, \pi/4\, D_{prop}^2} \quad (33)$$

where D_{prop} is the propeller diameter. The theoretical slipstream radius far aft of the propeller is:

$$r_{slip}^{\infty} \;\; = \;\; r_{prop} \; \sqrt{\frac{1}{2} \left(1 \; + \; \frac{U \; (1 \; - \; \tilde{w}_{prop})}{u_{slip}^{\infty}} \right)} \tag{34}$$

where r_{prop} is the propeller radius. The slipstream radius based on potential flow varies with longitudinal location as follows:

$$r_{slip}^{pot}(x) \;\; = \;\; r_{prop} \; \frac{0.14 \; \left(r_{slip}^{\infty}/r_{prop} \right)^3 \; + \; r_{slip}^{\infty}/r_{prop} \times [(x_{prop} - x)]^{1.5}}{0.14 \left(r_{slip}^{\infty}/r_{prop} \right)^3 \; + \; [(x_{prop} - x) \, / r_{prop}]^{1.5}} \tag{35}$$

Similarly the slipstream velocity based on potential flow varies with longitudinal location as follows:

$$u_{slip}^{pot}(x) \;\; = \;\; u_{slip}^{\infty} \; \left(\frac{r_{slip}^{\infty}}{r_{slip}^{pot}(x)} \right)^2 \tag{36}$$

Due to turbulence effects, corrections to both the slipstream radius and velocity can be made as follows:

$$r_{slip}(x) \;\; = \;\; r_{slip}^{pot}(x) \; + \; 0.15 \left(x_{prop} - x \right) \frac{u_{slip}^{pot}(x) \; - \; U \; (1 \; - \; \tilde{w}_{prop})}{u_{slip}^{pot}(x) \; + \; U \; (1 \; - \; \tilde{w}_{prop})}$$

$$u_{slip}(x) \;\; = \;\; u_{slip}^{pot}(x) + \left[u_{slip}^{pot}(x) - U \, (1 - \tilde{w}_{prop}) \right] \left(\frac{r_{slip}^{pot}(x)}{r_{slip}(x)} \right)^2 \; + \; U \, (1 - \tilde{w}_{prop}) \tag{37}$$

The lateral and vertical velocity components of the rudder are evaluated as follows:

$$v_r \;\; = \;\; \dot{\eta}_2 \; + \; x_{lift} \, \dot{\eta}_6 \tag{38}$$

$$w_r \;\; = \;\; \dot{\eta}_3 \; - \; x_{lift} \, \dot{\eta}_5 \tag{39}$$

When evaluating the effective incident flow acting on a rudder, a flow straightening coefficient γ_r is often applied [9, 11, 12, 13]. The flow straightening coefficient accounts for the influence of the hull, and typically has a value of less than one, meaning that the cross-flow velocity is reduced due to the presence of the hull. Lewandowski [11] gives the following equation for estimating the flow straightening coefficient:

$$\gamma_r \;\; \approx \;\; \frac{1}{1 \; + \; C_B} \tag{40}$$

where C_B is the ship hull block coefficient. Incorporating the effect of the flow straightening coefficient, the effective total velocity of the rudder relative to the incident flow is given by the following:

$$V_r \;\; = \;\; \sqrt{u_r^2 \; + \; \gamma_r^2 \; \left(v_r^2 \sin^2 \Gamma_r \; + \; v_r^2 \cos^2 \Gamma_r \right)} \tag{41}$$

where Γ_r is the dihedral angle of the rudder, as shown in Figure 7. The dihedral angle for a typical rudder is $-90°$. Note that terms with Γ_r in Equation (41) cause the spanwise component of flow to be excluded when evaluating V_r.
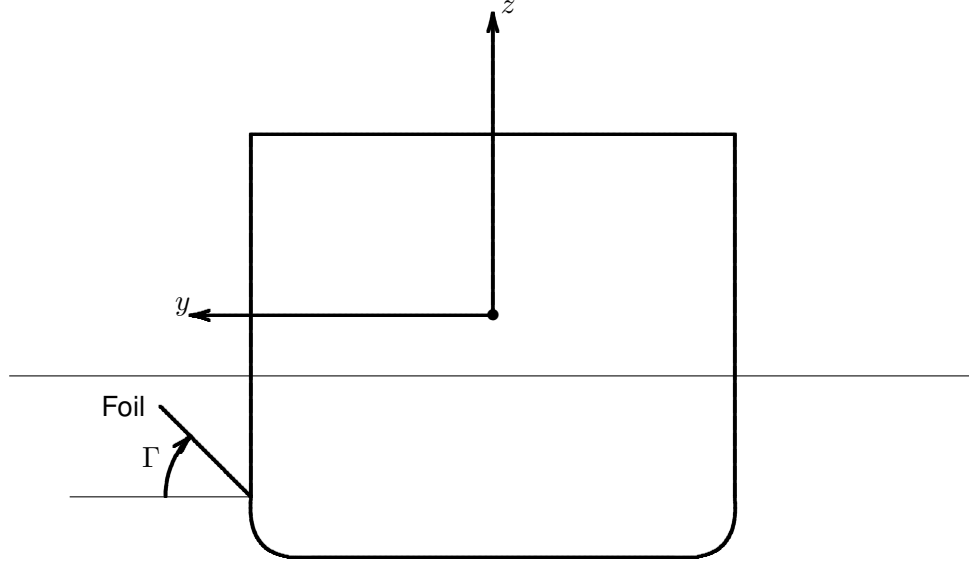
Figure 7: *Dihedral Angle Γ for Rudders and Other Foils*

The flow angle of attack α acting on the rudder includes contributions from both the rudder deflection δ^{rudder} and the incident flow. ShipMo3D uses a rudder deflection convention of positive for counter-clockwise rotation when viewed from inside the ship. Using this convention, the total angle of attack on a rudder is expressed as:

$$\alpha = \delta^{rudder} + \alpha_{V_r} \tag{42}$$

The angle of attack of the incident flow relative to the x axis is given by:

$$\alpha_{V_r} = \gamma_r \left[\left(\arctan \frac{v_r}{u_r} - \eta_6 \right) \sin \Gamma_r - \left(\arctan \frac{w_r}{u_r} + \eta_5 \right) \cos \Gamma_r \right] \tag{43}$$

Knowing the incident flow characteristics, the lift and drag forces acting on the rudder can be computed using Equations (27) and (28), and the forces acting on the ship can then be given by:

$$F_1 = F_{lift}^{rudder} \sin \alpha_{V_r} - F_{drag}^{rudder} \cos \alpha_{V_r} \tag{44}$$

$$F_2 = \left(-F_{lift}^{rudder} \cos \alpha_{V_r} - F_{drag}^{rudder} \sin \alpha_{V_r} \right) \sin \Gamma_r \tag{45}$$

$$F_3 = \left(-F_{lift}^{rudder} \cos \alpha_{V_r} - F_{drag}^{rudder} \sin \alpha_{V_r} \right) \cos \Gamma_r \tag{46}$$

$$F_4 = -z\,F_2 + y\,F_3 \qquad (47)$$

$$F_5 = z\,F_1 - x\,F_3 \qquad (48)$$

$$F_6 = -y\,F_1 + x\,F_2 \qquad (49)$$

As mentioned previously, the above formulation gives forces in translating earth axes assuming small amplitude motions. Within ShipMo3D, large amplitude motion effects are included by computing forces in ship-based axes and transforming values to translating earth axes.

The above discussion of rudder forces does not include lift forces due to a seaway. Due to uncertainties regarding interactions between the seaway, rudder, and propeller, lift forces due to the seaway are still evaluated without considering the influence of the propeller, as was originally done in Reference 3. The influence of this simplification will likely be minor because wave-induced water particle velocities will typically be small relative to velocities related to ship maneuvering.

5 Introduction of a Proportional-Integral-Derivative Autopilot

Due to its widespread usage onboard ships, a proportional-integral-derivative (PID) autopilot has been implemented within ShipMo3D. Fossen [19] gives a comprehensive treatment of PID and other autopilot types for marine vehicles.

The command rudder angle δ_C^{rudder} given by a PID autopilot is as follows:

$$\delta_C^{rudder} = \sum_{j=1}^{6} \left[k_{\delta j}^P \left(\eta_j^f - \eta_{Cj}^f \right) + k_{\delta j}^I \int_0^{\tau_{max}^{rudder}} \left(\eta_j^f(t-\tau) - \eta_{Cj}^f \right) d\tau + k_{\delta j}^D \dot{\eta}_j^f \right] \quad (50)$$

where $k_{\delta j}^P$ is the proportional gain for mode j, η_j^f is the motion displacement in earth-fixed axes for mode j, η_{Cj}^f is the command motion displacement for mode j, $k_{\delta j}^I$ is the integral gain for mode j, τ_{max}^{rudder} is the integration duration, t is the current time, τ is the time delay for integration, $k_{\delta j}^D$ is the derivative gain for mode j, and $\dot{\eta}_j^f$ is the motion velocity in earth-fixed axes for mode j. For a given command rudder angle δ_C^{rudder}, which can be provided by the autopilot or by a helmsman, the rudder response is modelled as follows:

$$\ddot{\delta}^{rudder} + 2\,\zeta_\delta\,\omega_\delta^{rudder}\,\dot{\delta}^{rudder} + \omega_\delta^2\,\delta^{rudder} = \omega_\delta^2\,\delta_C^{rudder} \qquad (51)$$

where ζ_δ is the nondimensional damping response constant, and ω_δ is the rudder frequency response constant.

6 Turning Circle Predictions for the Tanker Esso Osaka

Turning circle predictions have been performed for the Esso Osaka, an oil tanker that has been the subject of extensive maneuvering studies in the open literature [9, 20]. Table 1 gives main particulars for the Esso Osaka. ShipMo3D predictions for the Esso Osaka were originally presented in Reference 4.

Table 1: Main Particulars for the Esso Osaka During Maneuvering Trials

Length, L (between perpendiculars)	$325\,\mathrm{m}$
Beam, B	$53\,\mathrm{m}$
Midships draft, T_{mid}	$21.73\,\mathrm{m}$
Trim by stern, t_{stern}	$0.0\,\mathrm{m}$
Displacement, $\triangle$	$319{,}400\,\mathrm{tonnes}$
Longitudinal CG forward of midship	$10.3\,\mathrm{m}$

6.1 ShipMo3D Models of the Esso Osaka

Two models of the Esso Osaka were developed using the ShipMo3D applications SM3DPanelHull, SM3DRadDif, and SM3DBuildShip, which are described in Reference 6. The first ShipMo3D model of the Esso Osaka uses experimental hull maneuvering force coefficients, while the second model uses predicted hull maneuvering force coefficients based on Inoue et al. [10]. Both of the ship models include modifications to evaluation of hull maneuvering forces and rudder forces described earlier in this report. Figure 8 shows a ShipMo3D model of the Esso Osaka.

The ship model based on experimental hull maneuvering coefficients uses values for a bare hull model reported in Table 5.2 of the ITTC Esso Osaka Committee report [9]. Some of the nonlinear hull force coefficients in the ITTC report have a different format to those developed by Inoue et al. that are used within ShipMo3D. Where differences occur, equivalent ShipMo3D coefficients can be obtained as follows:

$$Y'_{v|v|} = Y'_{vvv}\ |v'_{nom}| \tag{52}$$

$$Y'_{v|r|} = Y'_{vrr}\ |r'_{nom}| \tag{53}$$

$$Y'_{r|r|} = Y'_{rrr}\ |r'_{nom}| \tag{54}$$

$$N'_{r|r|} = N'_{rrr}\ |r'_{nom}| \tag{55}$$

where Y'_{vvv}, Y'_{vrr}, Y'_{rrr}, and $N'_{r|r|}$ are nonlinear hull force coefficients reported by the ITTC, v'_{nom} is the nominal non-dimensional sway velocity for matching nonlinear
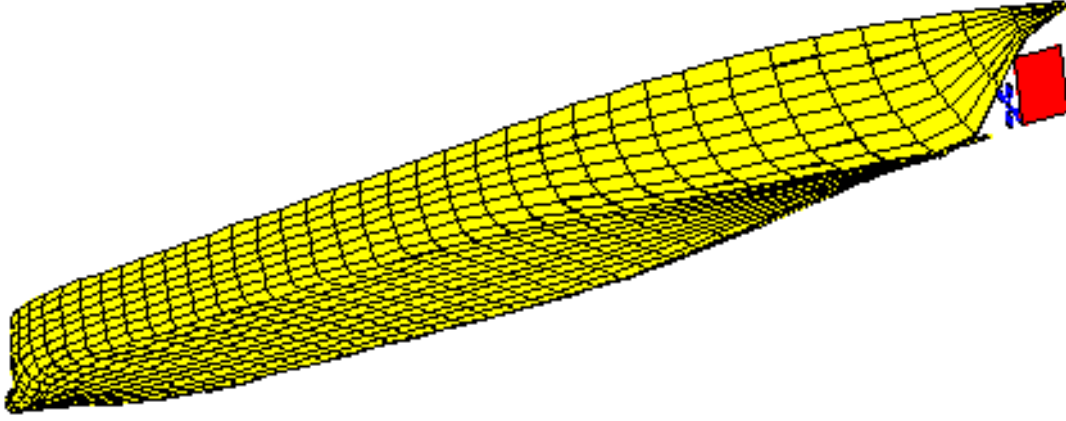
Figure 8: *ShipMo3D Model of Esso Osaka Including Panelled Wet Hull, Propeller, and Rudder*

forces from the Inoue et al. and ITTC formulations, and r'_{nom} is the nominal non-dimensional yaw velocity for matching nonlinear forces. The ShipMo3D coefficients were obtained using turning circle characteristics for the Esso Osaka with an initial speed of 10 knots, resulting in an equilibrium condition with a final total speed of 3.5 knots, yaw rate of 0.3 degrees per second, and drift angle of 15°, giving $|v'_{nom}| = 0.262$ and $|r'_{nom}| = 0.944$.

For the linear sway-yaw force coefficient, Table 5.2 of Reference 9 gives $Y'_r - m'_x$, which includes the nondimensional surge added mass. Radiation computations with ShipMo3D indicate that the nondimensional surge added mass for the Esso Osaka has a value of 0.016 at zero forward speed and zero motion frequency, which has been considered when evaluating an input Y'_r value for ShipMo3D.

When using experimental hull coefficients as input to ShipMo3D, they should be referenced to the ship centre of gravity (CG). Table 5.2 of Reference 9 gives hull coefficients based on motions at the CG and forces relative to midships. To obtain forces relative to the CG for ShipMo3D, the following corrections have been applied:

$$N'_v(CG, CG) \;=\; N'_v(mid, CG) \;+\; \frac{x_{mid}}{L}\, Y'_v(mid, CG) \tag{56}$$

$$N'_r(CG, CG) \;=\; N'_r(mid, CG) \;+\; \frac{x_{mid}}{L}\, Y'_r(mid, CG) \tag{57}$$

$$\tag{58}$$

where $N'_v(CG, CG)$ and $N'_r(CG, CG)$ are hull force coefficients with both forces and motions referenced to the CG, $N'_v(mid, CG)$, $Y'_v(mid, CG)$, $N'_r(mid, CG)$, and $Y'_r(mid, CG)$ are hull force coefficients with forces referenced to midships and motions referenced to the CG, and x_{mid} is the x coordinate of midships relative to the

CG. Note that the sway force terms $Y_v'(mid, CG)$ and $Y_r'(mid, CG)$ require no corrections to obtain values with forces referenced to the ship CG. For nonlinear hull force terms, it is assumed that corrections of force coefficients to be relative to the CG are negligible.

Table 2 shows generally good agreement between predicted and experimental hull force coefficients. The experimental coefficients in Table 2 are given for both forces and motions relative to the CG. For the predicted hull force coefficients based on Inoue et al., no corrections have been applied to transfer force and motion locations from midships to the CG because the magnitude of such corrections would be small relative to the uncertainties in predicted hull force coefficients. When comparing the hull force coefficients in Table 2, the most notable differences are for the terms $Y_{r|r|}'$ and N_{vr^2}', which both have predicted values of 0.0.

Table 2: *Esso Osaka Hull Force Coefficients from Experiments [9] and Predicted Using Inoue et al. [10]*

	Experiments	Predicted
Sway-sway		
Y_v'	-0.383	-0.400
$Y_{v|v|}'$	-0.276	-0.360
$Y_{v|r|}'$	-0.242	-0.317
Sway-yaw		
Y_r'	0.098	0.105
$Y_{r|r|}'$	-0.011	0.0
Yaw-sway		
N_v'	-0.135	-0.134
N_{vr^2}'	0.024	0.000
Yaw-yaw		
N_r'	-0.051	-0.054
N_{rv^2}'	-0.297	-0.200
$N_{r|r|}'$	-0.017	-0.012

The resistance and propulsion characteristics for the Esso Osaka were assumed to be the same as from the previous ShipMo3D maneuvering study [4]. Table 3 gives

Table 3: *Estimated Resistance Coefficients for Esso Osaka*

Speed (knots)	Resistance coefficient $C_{Dx} = F/(1/2\rho U^2 A_w)$
2.0	0.00306
16.0	0.00306
18.0	0.00308
19.6	0.00328
21.2	0.00370
22.9	0.00426

estimated resistance coefficients based on the Series 60 hull with a block coefficient of 0.80 [21], which has a geometry very similar to the Esso Osaka. Based on data given in Reference 22, the wake fraction $\tilde{w}_{prop}$ was estimated to be 0.352 and the thrust deduction coefficient t_{prop} was estimated to be 0.2. The Esso Osaka has a propeller diameter of 9.1 m. The following thrust coefficient curve was obtained by scaling a reference curve to match the reported full-scale speed of 10 knots with a propeller speed of 51 RPM.

$$K_T = 0.394 - 0.197\,J_{prop} - 0.148\,J_{prop}^2 \tag{59}$$

Table 4 gives rudder dimensions, autopilot parameters, and hydrodynamic coefficients. The rudder wake fraction and flow straightening coefficient are based on reported values in Reference 9. The rudder-propeller interaction coefficient is based on the ratio of the propeller diameter to the rudder span, and represents an estimate of the fraction of the rudder within the propeller slipstream.

6.2 Comparisons of Predicted and Measured Turning Circles

Figures 9 to 14 show comparisons of predicted and measured turning circles for the Esso Osaka. When considering the measured turning circles, it should be noted that scatter is greater for the lower speed of 7.7 knots, likely due to the greater susceptibility to environment forces at lower ship speed. During the initial stages of each turning circle, both sets of predictions agree closely with the measured results. Differences among the measured results and two sets of predictions increase as the turn radius decreases, which is expected because nonlinear forces, which are difficult to predict, become more important. Of the two sets of predictions, the predictions based on the

Table 4: *Rudder Dimensions, Autopilot Parameters, and Hydrodynamic Coefficients for Esso Osaka*

Rudder span s_{rudder}	$13.85\,\mathrm{m}$
Rudder chord length c_{rudder}	$9.00\,\mathrm{m}$
Maximum rudder deflection δ_{max}^{rudder}	35 degrees
Maximum rudder velocity $\dot{\delta}_{max}^{rudder}$	$3\,\mathrm{deg/s}$
Response natural frequency ω_δ	$3\,\mathrm{rad/s}$
Response damping ζ_δ	0.85
Rudder wake fraction $\tilde{w}_r$	0.0
Rudder flow straightening coefficient γ_r	0.4
Rudder-propeller interaction coefficient $C^{rudder-prop}$	0.66

experimental hull force coefficients appear to be better than the predictions based on hull coefficients estimated based on Inoue et al., as would be expected. The estimated hull coefficients give lower speed and higher yaw rates, resulting in noticeably smaller final turning radius.

Figure 9: *Esso Osaka Trajectory During Turning Circle, Initial Speed of 10 knots*

Figure 10: *Esso Osaka Total Speed During Turning Circle, Initial Speed of 10 knots*
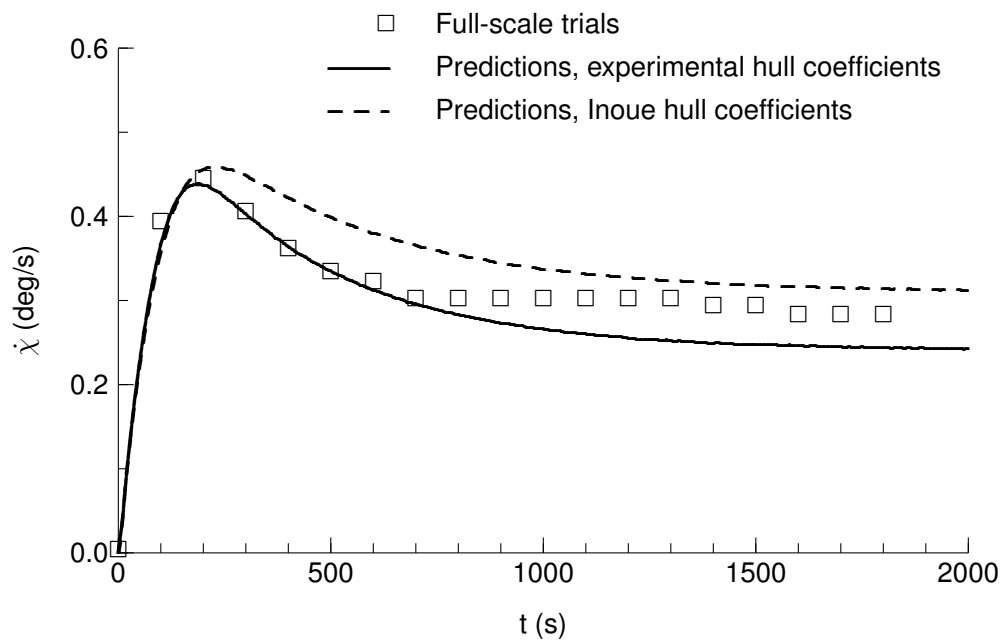
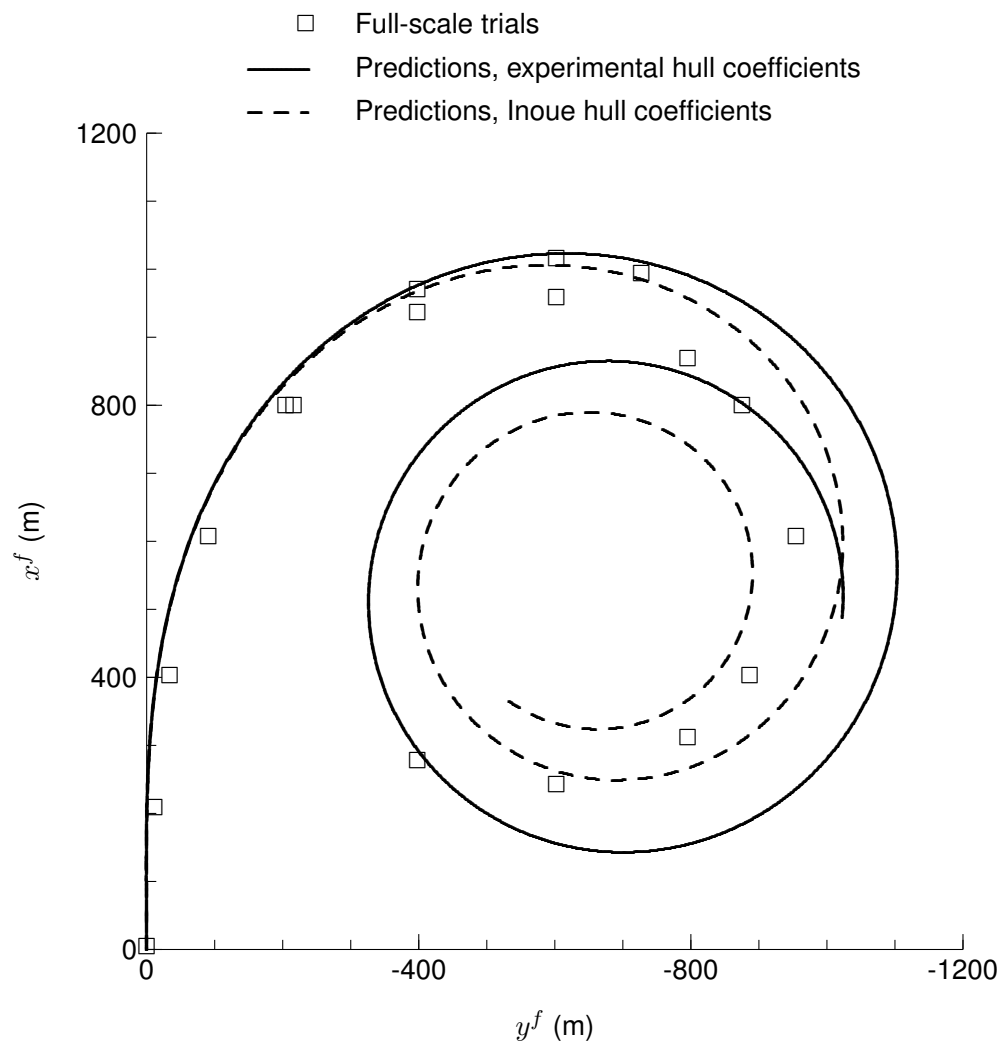**Figure 11:** *Esso Osaka Yaw Rate During Turning Circle, Initial Speed of 10 knots*

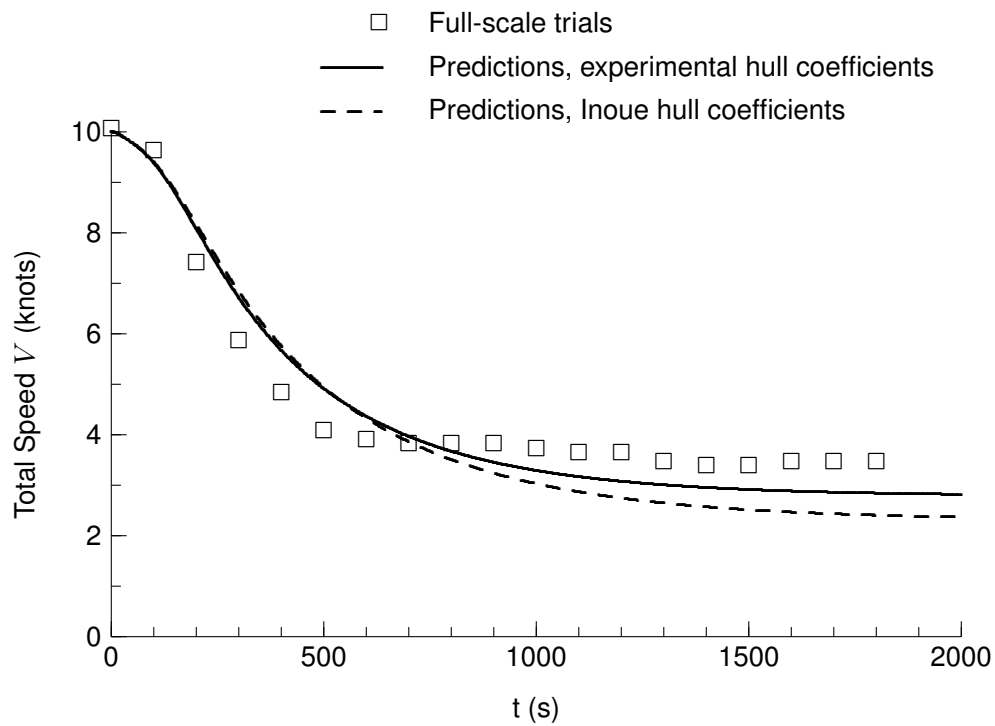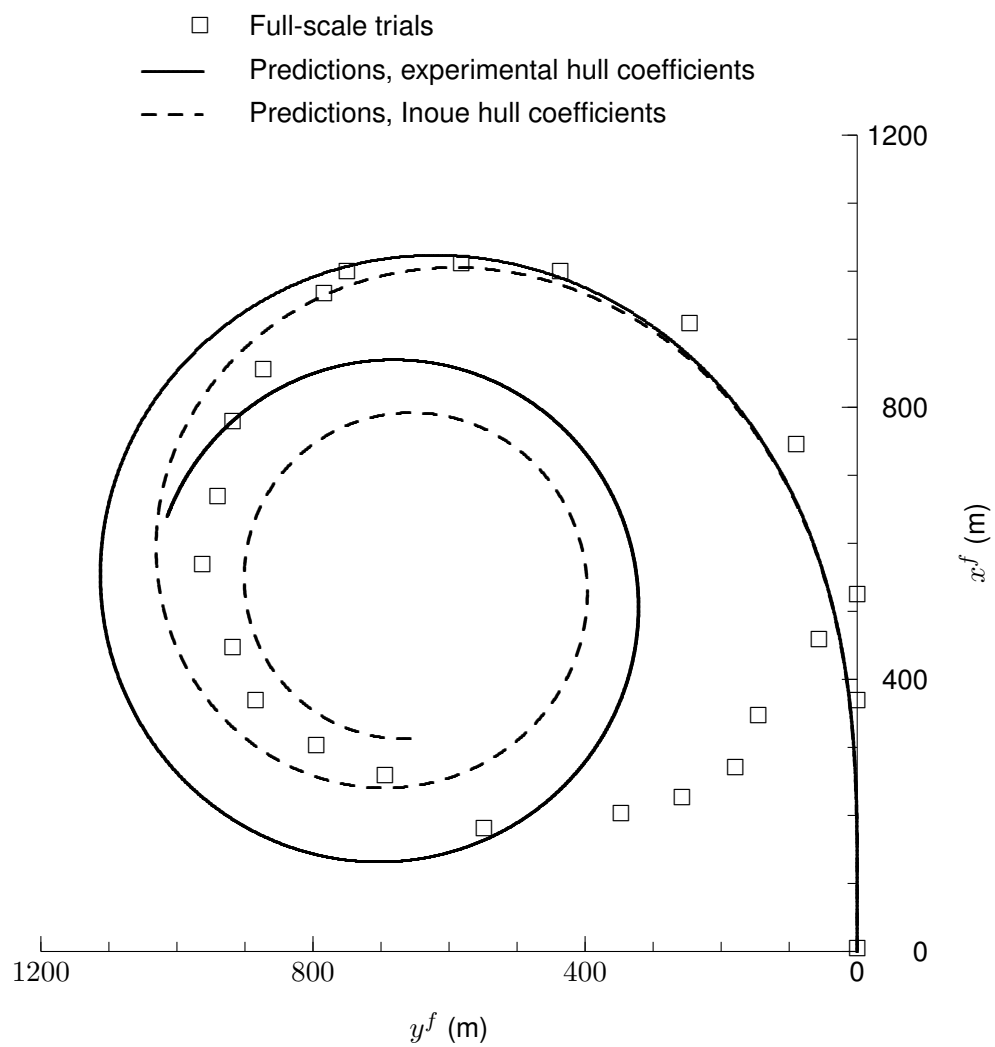**Figure 12:** *Esso Osaka Trajectory During Turning Circle, Initial Speed of 7.7 knots*
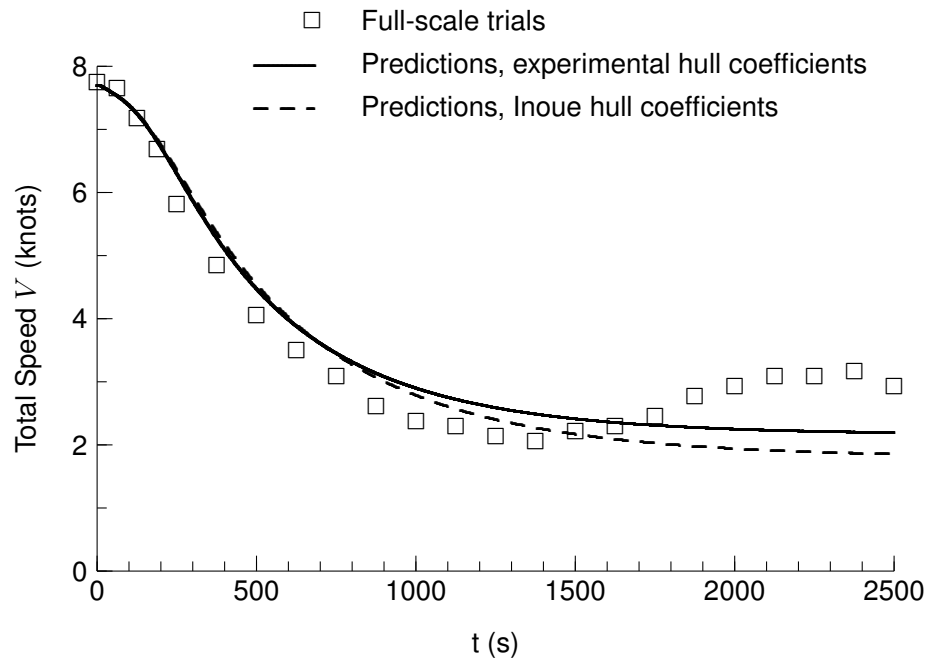
Figure 13: *Esso Osaka Total Speed During Turning Circle, Initial Speed of 7.7 knots*
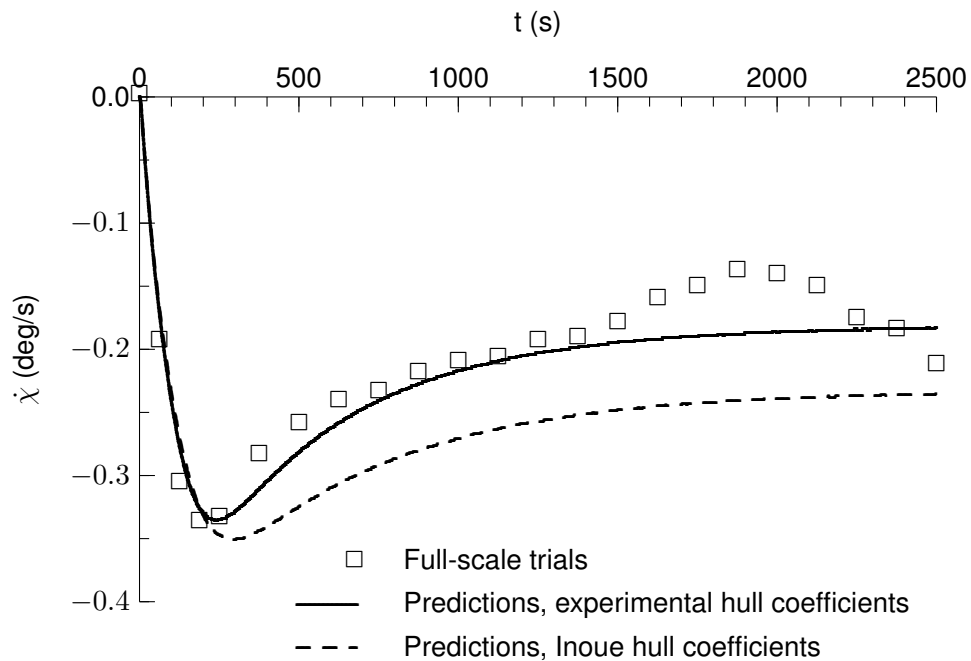
Figure 14: *Esso Osaka Yaw Rate During Turning Circle, Initial Speed of 7.7 knots*

7 Conclusions

Improvements have been made to evaluation of hull maneuvering forces and rudder forces within ShipMo3D. ShipMo3D also now has a new capability for modelling PID autopilots. Turning circle predictions for the tanker Esso Osaka show good agreement with sea trials data. Turning circle predictions based on experimental hull maneuvering coefficients are more accurate than predictions based on hull maneuvering coefficients estimated using the regression method of Inoue et al. [10].

References

[1] McTaggart, K. (2002), Three Dimensional Ship Hydrodynamic Coefficients Using the Zero Forward Speed Green Function, (DRDC Atlantic TM 2002-059) Defence Research and Development Canada - Atlantic.

[2] McTaggart, K. (2003), Hydrodynamic Forces and Motions in the Time Domain for an Unappended Ship Hull, (DRDC Atlantic TM 2003-104) Defence Research and Development Canada - Atlantic.

[3] McTaggart, K. (2004), Appendage and Viscous Forces for Ship Motions in Waves, (DRDC Atlantic TM 2004-227) Defence Research and Development Canada - Atlantic.

[4] McTaggart, K. (2005), Simulation of Hydrodynamic Forces and Motions for a Freely Maneuvering Ship in a Seaway, (DRDC Atlantic TM 2005-071) Defence Research and Development Canada - Atlantic.

[5] McTaggart, K. (2007), ShipMo3D Version 1.0 User Manual for Frequency Domain Analysis of Ship Seakeeping in a Seaway, (DRDC Atlantic TM 2007-171) Defence Research and Development Canada - Atlantic.

[6] McTaggart, K. (2007), ShipMo3D Version 1.0 User Manual for Simulating Motions of a Freely Maneuvering Ship in a Seaway, (DRDC Atlantic TM 2007-172) Defence Research and Development Canada - Atlantic.

[7] McTaggart, K. (2007), Validation of ShipMo3D Version 1.0 User Applications for Simulation of Ship Motions, (DRDC Atlantic TM 2007-173) Defence Research and Development Canada - Atlantic.

[8] Schmitke, R. (1978), Ship Sway, Roll, and Yaw Motions in Oblique Seas, *Transactions, Society of Naval Architects and Marine Engineers*, 86, 26–46.

[9] (2002), The Specialist Committee on Esso Osaka - Final Recommendations to the 23rd ITTC, In *23rd International Towing Tank Conference*, Vol. II, pp. 573–609, The Hague.

[10] Inoue, S., Hirano, M., and Kijima, K. (1981), Hydrodynamic Derivatives on Ship Manoeuvring, *International Shipbuilding Progress*, 28(321), 112–125.

[11] Lewandowski, E. M. (2004), The Dynamics of Marine Craft - Maneuvering and Seakeeping, Vol. 22 of *Advanced Series on Ocean Engineering*, River Edge, New Jersey: World Scientific.

[12] Faltinsen, O. (2005), Hydrodynamics of High-Speed Marine Vehicles, Cambridge, United Kingdom: Cambridge University Press.

[13] Inoue, S., Hirano, M., Kijima, K., and Takashina, J. (1981), A Practical Calculation Method of Ship Manoeuvring Motion, *International Shipbuilding Progress*, 28(325), 207–222.

[14] Newman, J. (1977), Marine Hydrodynamics, Cambridge, Massachusetts: MIT Press.

[15] Whicker, L. and Fehlner, L. (1958), Free Stream Characteristics of a Family of Low Aspect Ratio Control Surfaces for Application to Ship Design, (Report DTRC 933) David Taylor Research Center.

[16] Bertram, V. (2000), Practical Ship Hydrodynamics, Oxford: Butterworth-Heinemann.

[17] Söding, H. (1982), Prediction of Ship Steering Capabilities, *Schiffstechnik (Ship Technology Research)*, 29, 3–29.

[18] Söding, H. (1998), Limits of Potential Theory in Rudder Flow Predictions, In *22nd Symposium on Naval Hydrodynamics*, Washington.

[19] Fossen, T. (1994), Guidance and Control of Ocean Vehicles, Chichester: John Wiley & Sons.

[20] Crane, C., Jr. (1979), Maneuvering Trials of the 278,000 DWT Esso Osaka in Shallow and Deep Water, *Transactions, Society of Naval Architects and Marine Engineers*, Vol. 87.

[21] Todd, F. (1953), Some Further Experiments on Single-Screw Merchant Ship Forms - Series 60, *Transactions, Society of Naval Architects and Marine Engineers*, 61, 516–589.

[22] van Manen, J. and van Oossanen, P. (1988), Principles of Naval Architecture, Volume II, Ch. 6, Propulsion, Society of Naval Architects and Marine Engineers.

Symbols and Abbreviations

$[A]$	added mass matrix
$[A^{bk-i}]$	added mass matrix of bilge keel i
$[A^{foil-i}]$	added mass matrix of foil i
$[A^{hull}]$	hull added mass matrix
$\partial \widetilde{A}_{jk}^{hull}/\partial x$	term based on x derivatives of added mass potentials
$[A^{rudder-i}]$	added mass matrix of rudder i
$[A^{skeg-i}]$	added mass matrix of skeg i
a_e	effective aspect ratio of foil
B	ship beam
$[B]$	damping matrix
$[B^{bk-i}]$	damping matrix of bilge keel i
$[B^{foil-i}]$	damping matrix of foil i
$[B^{hull-man}]$	hull maneuvering damping matrix
$[b^{hull-rad}]$	frequency-independent damping matrix due to potential flow
$[B^{hull-visc}]$	hull viscous damping matrix
$[B^{skeg-i}]$	damping matrix of skeg i
$B_{22V}^{hull-man}$	sway-sway linear maneuvering coefficient
$B_{22V|r'|}^{hull-man}$	sway-sway maneuvering coefficient for yaw nonlinearity
$B_{22V|v'|}^{hull-man}$	sway-sway maneuvering coefficient for sway nonlinearity
$B_{26V}^{hull-man}$	sway-yaw linear maneuvering coefficient
$B_{26V|r'|}^{hull-man}$	sway-sway maneuvering coefficient for yaw nonlinearity
$B_{62V}^{hull-man}$	yaw-sway linear maneuvering coefficient
$B_{62V|r'^2|}^{hull-man}$	yaw-sway maneuvering coefficient for yaw nonlinearity
$B_{66V}^{hull-man}$	yaw-yaw linear maneuvering coefficient
$B_{66V|r'|}^{hull-man}$	yaw-yaw maneuvering coefficient for yaw nonlinearity
$B_{66V|v'^2|}^{hull-man}$	yaw-yaw maneuvering coefficient for sway nonlinearity
$B_{22U}^{hull-rad-stab}$	sway-sway radiation damping term
$B_{26U}^{hull-rad-stab}$	sway-yaw radiation damping term
$B_{62U}^{hull-rad-stab}$	yaw-sway radiation damping term
$B_{66U}^{hull-rad-stab}$	yaw-yaw radiation damping term
C_B	ship block coefficient
C_{Dx}	hull resistance coefficient
$[C^{bk-i}]$	stiffness force matrix for bilge keel i

$[C^{buoy}]$	hull buoyancy stiffness matrix
C^{drag}	foil drag force coefficient
$[C^{foil-i}]$	stiffness force matrix for foil i
$C_j^{rudder-prop}$	rudder-propeller interaction coefficient from propeller j
$[C^{hull-man}]$	hull maneuvering force stiffness matrix
C^{lift}	foil lift force coefficient
$[C^{skeg-i}]$	stiffness force matrix for skeg i
C_{th}	propeller thrust loading coefficient
CG	centre of gravity
$\bar{c}$	mean chord length
$[c^{hull}]$	hull frequency-independent stiffness due to potential flow
D_{prop}	propeller diameter
F_j	force component for mode j in translating earth axes
$\{F^D\}$	wave diffraction force vector
$\{F^I\}$	incident wave excitation force vector
$\{F^{I-bk-i}\}$	incident wave force vector on bilge keel i
$\{F^{I-foil-i}\}$	incident wave force vector on foil i
$\{F^{I-hull}\}$	incident wave force vector on hull
$\{F^{I-skeg-i}\}$	incident wave force vector on skeg i
F_{lift}^{drag}	rudder drag force
F_{lift}^{rudder}	rudder lift force
F^{prop}	propeller thrust
$\{F^{rudder-i}\}$	non-inertial force vector on rudder i
F_j^S	force component for mode j in ship-based axes
J_{prop}	propeller advance ratio
K_T	propeller thrust coefficient
$[K^{hull}]$	retardation function matrix
$k_{\delta j}^D$	autopilot derivative gain for mode j
$k_{\delta j}^I$	autopilot integral gain for mode j
$k_{\delta j}^P$	autopilot proportional gain for mode j
L	ship length between perpendiculars
$[M]$	ship inertia matrix
m_x'	nondimensional surge added mass
N_r'	non-dimensional yaw-yaw maneuvering force coefficient

$N'_{r\|r\|}$	non-dimensional yaw-yaw maneuvering force coefficient with yaw non-linearity
N'_v	non-dimensional yaw-sway maneuvering force coefficient
r'	non-dimensional yaw velocity
r'_{nom}	nominal non-dimensional yaw velocity
r_{slip}	slipstream radius
r^∞_{slip}	slipstream radius far aft of propeller
S	foil area
s	foil span
T_{mid}	draft at midships
t	time
t_{stern}	trim by stern
U	ship forward speed
u_r, v_r, w_r	water relative velocity components
u_{slip-j}	slipstream velocity aft of propeller j
u^{pot}_{slip}	slipstream velocity aft of propeller based on potential flow
u^∞_{slip}	flow velocity far aft of propeller
V	total ship speed in horizontal plane
V_r	incident flow velocity on rudder
v'	non-dimensional sway velocity
v'_{nom}	nominal non-dimensional sway velocity
$\tilde{w}_{prop}$	propeller wake fraction
x_f, y_f	horizontal plane coordinates in earth-fixed axes
$\ddot{x}^f, \ddot{y}^f$	horizontal plane accelerations
Y'_r	non-dimensional sway-yaw maneuvering force coefficient
Y'_{rrr}	non-dimensional sway-yaw maneuvering force coefficient with yaw non-linearity
Y'_v	non-dimensional sway-sway maneuvering force coefficient
Y'_{vrr}	non-dimensional sway-sway maneuvering force coefficient with yaw non-linearity
Y'_{vvv}	non-dimensional sway-sway maneuvering force coefficient with sway nonlinearity
x_{lift}	longitudinal location of lift force
α	flow angle of attack
γ^r	rudder flow straightening constant
δ^{rudder}	rudder deflection angle

δ_{max}^{rudder}	maximum rudder deflection angle
$\dot{\delta}^{rudder}$	rudder deflection velocity
$\dot{\delta}_{max}^{rudder}$	maximum rudder deflection velocity
$\ddot{\delta}^{rudder}$	rudder deflection acceleration
δ_C^{rudder}	command rudder angle
ζ_δ	rudder control damping coefficient
η_j	motion displacement in translating earth axes for mode j
$\ddot{\eta}_j$	acceleration in translating earth axes for mode j
η_j^f	motion displacement in earth-fixed axes for mode j
η_{Cj}^f	command motion displacement in earth-fixed axes for mode j
$\dot{\eta}_j^f$	motion velocity in earth-fixed axes for mode j
ρ	water density
τ_{max}^{rudder}	autopilot integration duration
$\dot{\chi}$	yaw velocity in earth-fixed axes
$\ddot{\chi}$	yaw acceleration in earth-fixed axes
ω_e	encounter frequency
ω_δ	rudder control natural frequency
$\triangle$	ship mass displacement

Distribution List

LIST PART 1: Internal Distribution by Centre

1   Author (1 hard copy)

5   DRDC Atlantic Library (1 hard copy)

3   Project Officer ABCA-02-01 (CSci) for distribution

12   Project Officer ABCANZ-97-12 (H/WP) for distribution (12 hard copies)

21   TOTAL LIST PART 1 (7 CD, 14 HARD COPIES)

LIST PART 2: External Distribution by DRDKIM

1   Library and Archives Canada

1   DRDKIM 3

1   DMSS 2
     555 Blvd. De la Carriere
     Gatineau, Quebec
     K1A 0K2

1   Canadian Forces Maritime Warfare School
     Attention: Commanding Officer
     P.O. Box 99000 STN Forces,
     Halifax, N.S. B3K 5X5

1   Director General (1 hard copy)
     Defence R&D Canada - Toronto
     1133 Sheppard Avenue West
     P.O. Box 2000
     Toronto, Ontario
     M3M 3B9

1 Director-General
   Institute for Ocean Technology
   National Research Council of Canada
   P.O. Box 12093, Station A
   St. John's, Newfoundland
   A1B 3T5

1 Transport Canada / Marine Safety
   Tower C, Place de Ville
   330 Sparks Street, 11th Floor
   Ottawa, Ontario
   CANADA
   K1A ON8

2 Commanding Officer (2 hard copies)
   U.S. Coast Guard Research and Development Center
   1082 Shennecosett Road
   Groton, CT 06340-2602

1 Ministry of Defence
   Attn: Head, Naval Research
   Dept. of Naval Architecture and Marine Engineering and Development
   P.O. Box 20702
   2500 ES, The Hague
   The Netherlands

1 FOI Swedish Defence Research Agency
   Attn: Eva Dalberg
   Grindsjon Research Centre
   SE-147 25 Tumba
   Sweden

1   Department of Defence (Navy Office)
Attn: Director Naval Ship Design
Campbell Park Office CPI-505
Canberra ACT 2600
Australia

1   Document Exchange Centre
Defence Information Services Branch
Department of Defence
Campbell Park Offices CP2-5-08
Canberra ACT 2600 Australia

1   Bundesamt fur Wehrtechnik und Beschaffung - SG I 3
Postfach 7360
6057 Koblenz
Germany

1   Dr. John Duncan
Defence Equipment and Support
Abbey Wood
Mail Point 8014
BRISTOL BS34 8JH
UK

---

15   TOTAL LIST PART 2 (13 CD, 2 HARD COPIES)

36   TOTAL COPIES REQUIRED (20 CD, 16 HARD COPIES)

This page intentionally left blank.

DOCUMENT CONTROL DATA

(Security classification of title, abstract and indexing annotation must be entered when document is classified)

1. ORIGINATOR (the name and address of the organization preparing the document). Defence R&D Canada - Atlantic	2. SECURITY CLASSIFICATION (overall security classification of the document including special warning terms if applicable) UNCLASSIFIED

3. TITLE (The complete document title as indicated on the title page. Its classification should be indicated by the appropriate abbreviation (S,C,R or U) in parentheses after the title.) Improved Maneuvering Forces and Autopilot Modelling for the ShipMo3D Ship Motion Library

4. AUTHORS (Last name, first name, middle initial. If military, show rank, e.g. Doe, Maj. John E.) McTaggart, Kevin A.

5. DATE OF PUBLICATION (month and year of publication of document) September 2008	6a. NO. OF PAGES (total including Annexes, Appendices, etc). 46	6b. NO. OF REFS (total cited in document) 22

7. DESCRIPTIVE NOTES (The category of the document, e.g. technical report, technical note or memorandum. If appropriate, enter the type of report, e.g. interim, progress, summary, annual or final.) Technical Memorandum

8. SPONSORING ACTIVITY (the name of the department project office or laboratory sponsoring the research and development. Include address). Defence R&D Canada - Atlantic, PO Box 1012, Dartmouth, NS, Canada B2Y 3Z7

9a. PROJECT OR GRANT NO. (If appropriate, the applicable research and development project or grant number under which the document was written.) 11GV05	9b. CONTRACT NO. (if appropriate, the applicable number under which the document was written).

10a. ORIGINATOR'S DOCUMENT NUMBER (the official document number by which the document is identified by the originating activity. This number must be unique.) DRDC Atlantic TM 2008-162	10b. OTHER DOCUMENT NOs. (Any other numbers which may be assigned this document either by the originator or by the sponsor.)

11. DOCUMENT AVAILABILITY (any limitations on further dissemination of the document, other than those imposed by security classification) (X) Unlimited distribution ( ) Defence departments and defence contractors; further distribution only as approved ( ) Defence departments and Canadian defence contractors; further distribution only as approved ( ) Government departments and agencies; further distribution only as approved ( ) Defence departments; further distribution only as approved ( ) Other (please specify):

12. DOCUMENT ANNOUNCEMENT (any limitation to the bibliographic announcement of this document. This will normally correspond to the Document Availability (11). However, where further distribution (beyond the audience specified in (11) is possible, a wider announcement audience may be selected).

13. ABSTRACT (a brief and factual summary of the document. It may also appear elsewhere in the body of the document itself. It is highly desirable that the abstract of classified documents be unclassified. Each paragraph of the abstract shall begin with an indication of the security classification of the information in the paragraph (unless the document itself is unclassified) represented as (S), (C), (R), or (U). It is not necessary to include here abstracts in both official languages unless the text is bilingual).

ShipMo3D is an object-oriented library with associated user applications for predicting ship motions in calm water and in waves. Motion predictions are available in both the frequency domain and the time domain. For predictions in the frequency domain, a ship is assumed to travel with quasi-steady speed and heading in waves. For predictions in the time domain, the ship can be freely maneuvering in either calm water or in waves. This report describes improvements to evaluation of hull maneuvering forces and rudder forces. The report also describes the implementation of a proportional-integral-derivative (PID) autopilot within ShipMo3D.

14. KEYWORDS, DESCRIPTORS or IDENTIFIERS (technically meaningful terms or short phrases that characterize a document and could be helpful in cataloguing the document. They should be selected so that no security classification is required. Identifiers, such as equipment model designation, trade name, military project code name, geographic location may also be included. If possible keywords should be selected from a published thesaurus. e.g. Thesaurus of Engineering and Scientific Terms (TEST) and that thesaurus-identified. If it not possible to select indexing terms which are Unclassified, the classification of each should be indicated as with the title).

autopilot
drag
lift
maneuvering
rudder
ship motions

This page intentionally left blank.

Defence R&D Canada

Canada's leader in defence
and National Security
Science and Technology

R & D pour la défense Canada

Chef de file au Canada en matière
de science et de technologie pour
la défense et la sécurité nationale

DEFENCE **R&D** DÉFENSE

www.drdc-rddc.gc.ca